CRYSTAL GROWTH & DESIGN

Article

Cite This: Cryst. Growth Des. 2019, 19, 1954−1964

pubs.acs.org/crystal

Three-Dimensional Porous Architectures Based on $Mn^{II/III}$ Three-Blade Paddle Wheel Metallacryptates

Vittoria Marzaroli,[†] Giulia Spigolon,[‡] Giuseppe Lococciolo,[†,∥] Martina Quaretti,[†] Clarissa Salviati,[†] Jeff W. Kampf,[§] Giulia Licini,[‡] Luciano Marchiò,[†] Vincent L. Pecoraro,*[,§] and Matteo Tegoni*[,†]

[†]Department of Chemistry, Life Sciences, and Environmental Sustainability, University of Parma, Parco Area delle Scienze 11A, 43124 Parma, Italy

[‡]Department of Chemical Sciences, University of Padova, via Marzolo 1, 35131 Padova, Italy

[§]Department of Chemistry, University of Michigan, Ann Arbor, Michigan 48109-1055, United States

Supporting Information

ABSTRACT: Three metallacryptate supramolecular assemblies have been obtained using salicylhydroxamic acid derivatives (H_3L). The three ligands differ in the residue at the *para* position with respect to the hydroxamic function (−H, $-NH_2$, and −(4-pyridyl)). The core of these supramolecules correspond to the formula $[(Mn^{II})_2(Mn^{III})_9(\mu_3\text{-}O)_4(OAc)_3(Shi)_6]^{2+}$ (abbreviated as $Mn_{11}L_6$) in all three compounds. Additional acetate or hydroxide ions and DMF molecules are coordinated to the Mn^{III} ions. With L^{3-} = Shi^{3-} the $Mn_{11}L_6$ units assemble into a nonporous structure, where the metallacryptates are linked together through Na^I ions bridging between the units. Conversely, with L^{3-} = *p*-$aShi^{3-}$ (NH_2 group) and *p*-$pyShi^{3-}$ (4-pyridyl group) the units assemble in parallel chains and into a MOF-like structure, respectively. In both solids, a honeycomb porous architecture was obtained, where infinite channels run along the crystal structure. With *p*-$aShi^{3-}$, Na^I bridging ions and hydrogen bonds, provided by the presence of the amino group, characterize the interactions between the parallel chains of supramolecules. On the other hand, with *p*-$pyShi^{3-}$, the peripheral pyridyl groups point away from the metallacryptate units and are coordinated to available positions on Mn^{III} ions of neighboring molecules, with formation of a peculiar porous-coordination polymeric architecture.

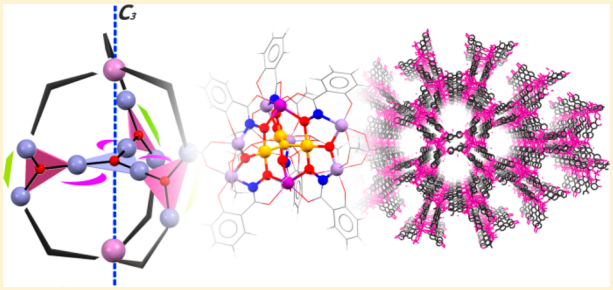

INTRODUCTION

There is great interest today in developing porous coordination polymers and, in general, large ordered assemblies of metal complexes.[1−6] These substances are promising materials that may have applications in gas storage, separations of small molecules, catalysis, luminescence, and magnetism.[7] For the construction of such materials, it is sometimes hard to predict the topology of the final architecture and to control the properties of the material. One successful approach for that purpose is constructing a 3D architecture, using preassembled polynuclear complexes, that exhibit at the molecular level the desired properties for the final material.[8,9]

Metallacrowns, the inorganic analogues of crown ethers, provide an opportunity to exploit these strategies for the construction of 3D architectures.[10−13] These metallamacrocyclic complexes are assembled from metal ions and bridging organic ligands such as hydroxamic acids and are characterized by the repetition of a cyclic $(M-N-O)_n$ connectivity (Scheme 1a). In metallacrowns, the oxygen atoms of the metallacycle point toward the center of the cavity, into which metal ions (from transition (d) to lanthanide (f) elements) can be encapsulated.[11,14,15] Closely related to metallacrowns are inverse metallacrowns and metallacryptates.[16−23] Inverse

Scheme 1. General Schematic Representations of the Metallacyclic Rings of Metallacrowns (a), Inverse Metallacrowns (b), and Inverse Metallacryptates (c)

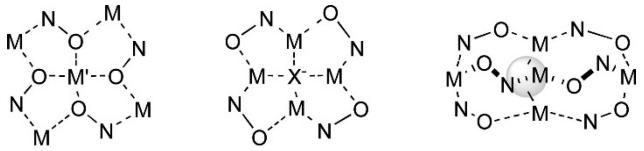

metallacrowns share with metallacrowns the cyclic repetition of a $(M-N-O)_n$ connectivity, but the conformation of the metallacyclic ring brings the metals rather than the oxygen to the interior point of the cavity (Scheme 1b).[16−19] In these constructs, the cavity is, therefore, occupied by anions such as oxide, hydroxide, or halogenides, which coordinate to the metal ions. More complex 3D assemblies using the same, or closely similar, $(M-N-O)_n$ repeating units can lead to metallacryptates, the inorganic analogues of cryptates. In

Received: December 27, 2018
Published: January 31, 2019

DOI: 10.1021/acs.cgd.8b01921
Cryst. Growth Des. 2019, 19, 1954−1964

these molecules, one can often discern interconnected metallacrown or inverse metallacrown motifs and connectivities that form a cage into which cations or anions are trapped (Scheme 1c).[20−23]

We have carried out in the past few years an extensive investigation of the functional properties of metallacrowns.[11,14,15,24,25] The most promising in terms of their possible applications are their luminescence brightness,[26−30] their single-molecule magnetic behavior,[21,31,40−42,32−39] and their selectivity as hosts for both anionic and cationic species.[43−51] These are all desirable properties to be incorporated into porous coordination polymers. Because metallacrowns are stable in solution over a wide range of conditions (e.g., pH, presence of competing ligands or metals, different solvents),[15,45,52] they serve as ideal building blocks for the assembly of 3D coordination polymers based on polymetallic species.[11,12,53] Metallacrowns can be preassembled in solution and, therefore, converted into the desired solid state architectures by variation in the conditions of crystallization. This capacity to give rise to coordination polymers has been documented.[54−63]

Several three-dimensional MC-based architectures have been presented in the literature in the past few years.[54−63] However, among these only a few were reported to possess real pores and none of them exhibited permanent porosity.[59,61] We have recently provided an important advancement in this field by reporting the preparation of the first three-dimensional coordination polymer based on an MC framework that exhibits permanent porosity.[10] This material was formed by Cu^{II}[12-$MC_{Cu,L}$-4] units, where the ligand L is a derivative of salicylhydroxamic acid, connected by Cu^{II} ions to form chessboard-like 2D layers that stack one above the other. The channels present in this framework have the capacity of being evacuated at high temperature and filled with gas molecules with no loss of crystallinity.[10]

More recently, efforts have been presented in the literature on making extended solids of materials that may have individual units with SMM and MOF behavior.[64−68] In view of obtaining these types of functional materials, we decided to move from copper to manganese assemblies. The latter can actually be more promising for revealing interesting magnetic properties, as a result of the great single ion paramagnetism and magnetic anisotropy.[69] In fact, the first documented single-molecule magnets (SMMs) were indeed collections of Mn^{III} and Mn^{IV}.[70,71] Furthermore, several metallacrowns and metallacryptates containing mixed-valence Mn assemblies have been shown to exhibit slow magnetic relaxation that is consistent with SMMs.[21,22,31,33−36] In this paper we present the synthesis of three salicylhydroximate derivatives (Shi^{3-}; Scheme 2) used to prepare self-assembled metallacryptate constructs which are 3-fold axially symmetric. On one hand, with all three ligands (H_3L) the obtained metallacryptate assemblies have the general stoichiometry $Mn_{11}L_6$ and they contain both Mn^{II} and Mn^{III} ions. These molecules are the first examples of [2.2.2]metallacryptates and are among the very few metallacryptates isolated to date.[20−23] Perhaps more importantly, by rational design of the ligand derivatives the 3-fold symmetry of these molecules was fully exploited to obtain three new 3D frameworks, among which two are porous. By X-ray structural characterization we demonstrated how a modification of the ligand by one atom on the aromatic ring of Shi^{3-} converts this molecular species into a 3D array, allowing us to move from a nonporous molecular packing to honeycomb-like architectures where infinite channels run along the crystal structure.

Scheme 2. Representation of H_3Shi (a) and Its Two Derivatives H_3*p*-aShi (b, 5) and H_3*p*-pyShi (c, 10)

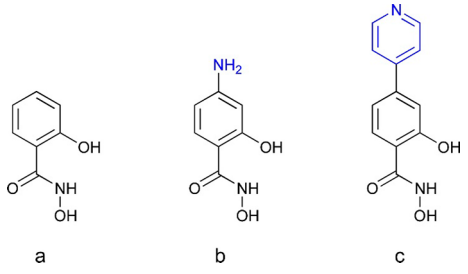

EXPERIMENTAL SECTION

Materials and Methods. Chemicals were purchased from Sigma-Aldrich and TCI Chemicals and used without further purification. Reactions performed under an inert atmosphere were carried out using Schlenk glassware with nitrogen as the inert gas. Flash column chromatography was performed using silica gel (230−400 mesh). Melting points were recorded with a Stuart SMP11 Melting Point instrument. ^{1}H and $^{13}C\{^1H\}$ NMR spectra were recorded on Bruker Avance-DPX-200, Bruker Avance 400, Varian MR400, and Varian Vnmrs500 spectrometers using standard pulse sequences. Chemical shifts were referenced to the residual signals of the solvents. The $^{13}C\{^1H\}$ NMR spectra (50 MHz) were referenced to the $CDCl_3$ peak. The following abbreviations are used in reporting the multiplicity for NMR resonances: s = single, d = doublet, dd = doublet of doublets, t= triplet, and m = multiplet. FT -IR spectra were recorded with a PerkinElmer FTIR 1650 or a PerkinElmer FTIR Nexus spectrometer using a Smart Orbit HATR accessory equipped with a diamond crystal. Electrospray ionization mass spectra (ESI-MS) of compounds **2−5** were collected on a Micromass LCT TOF electrospray ionization mass spectrometer, using a capillary voltage of 3500 V and a desolvation temperature of 350 °C. Samples (40 μM) were injected through direct infusion using a syringe pump at 11 μL/min, and the spectra were recorded in full scan analysis mode in the range m/z 100−2000. High-resolution electrospray ionization mass spectrometry HRMS (ESI-QTOF) analyses of compounds **6−10** were performed with a Waters Xevo G2-S QTof instrument in positive and negative mode (50/50 water/acetonitrile mixture with 0.1% of formic acid as mobile phase) with the following settings: solvent flow 50 μL/min, dry gas 800 L/h, dry temperature 350 °C, detector potential 2 kV. The MS peak intensity for each analysis is reported as monoisotopic mass, and the data were processed with Mass-Lynx 4.1.

X-ray Crystallography. Single-crystal X-ray diffraction data of **11** were collected at 293 K on a Bruker Smart APEXII CCD diffractometer (Mo Kα; λ = 0.71073 Å). Intensities were integrated from several series of exposure frames that covered the sphere of reciprocal space.[72] Single-crystal X-ray diffraction data of metallacryptates **12** and **13** were collected with a Rigaku AFC10K Saturn 944+ CCD-based X-ray diffractometer equipped with a low-temperature device and Micromax-007HF Cu-target microfocus rotating anode (λ = 1.54187 A) operated at 1.2 kW power (40 kV, 30 mA). Rigaku d*trek images were exported to CrysAlisPro for processing.[73] Absorption correction was applied using the program SADABS.[74] The data collection for **12bis** was performed at the X-ray diffraction beamline (XRD1) of the Elettra Synchrotron, Trieste, Italy.[75] Data sets were collected at 100 K through the rotating crystal method. Data were acquired using a monochromatic wavelength of 0.700 Å on a Pilatus 2 M hybrid-pixel area detector. The collected images were processed with CrysAlisPro.[73] The structures of compounds **11−13** were solved by direct methods with ShelXT[76] and refined with full-matrix least squares,[77] using the Olex2 software package. The structures were analyzed with the Mercury 3.10 software

DOI: 10.1021/acs.cgd.8b01921
Cryst. Growth Des. 2019, 19, 1954−1964

package.[78] Crystallographic data for **11**−**13** and for **12bis** reported in this paper have been deposited with the Cambridge Crystallographic Data Centre (CCDC deposition numbers: 1849184−1849186 and 1884452).

Synthesis of *N-tert*-Butyloxycarbonyl-4-aminosalicylic Acid (2). 4-Aminosalicylic acid (**1**; 4.0 g, 0.026 mol) was dissolved in 50 mL of ethanol. Sodium hydroxide (2.1 g, 0.052 mol), dissolved in 20 mL of water, was added. Di-*tert*-butyl dicarbonate (11.4 g, 0.052 mol), dissolved in 40 mL of ethanol, was added dropwise within 1 h, and the solution was stirred overnight. The solvent was removed in vacuo, and hydrochloric acid (1 M) was added up to pH 3. The precipitate was filtered off, washed with water, and dried under reduced pressure at room temperature to obtain a white powder (yield 3.7 g, 93%). FT-IR (ATR, cm^{-1}): 3361, 2884, 1737, 1621, 1588, 1452, 1298, 1220, 1192, 1138, 1048, 1023, 984, 914, 872, 826, 775, 699, 643, 596, 540, 504, 464. ^1H NMR (400 MHz, δ, DMSO-d_6) 9.71 (1H, s, Ar-NH), 7.64 (1H, d, J = 8.7 Hz, Ar-6H), 7.12 (1H, d, J = 2.1 Hz, Ar-3H), 6.98 (1H, dd, J = 8.8, J = 2.1 Hz, Ar-1H), 1.47 (9H, s, Boc-CH_3). ESI-MS (QTOF, m/z): 276.25 ($[M + Na]^+$), 292.21 ($[M + K]^+$); Anal. Found: C, 56.8; H, 6.2; N, 5.6. Calcd for $C_{12}H_{15}NO_5$: C, 56.9; H, 6.0; N, 5.5.

Synthesis of *N-tert*-Butyloxycarbonyl-4-aminosalicyl-*O*-benzylhydroxamate (3). Compound **2** (5.00 g, 0.0198 mol) was dissolved in 120 mL of DMF. Triethylamine (5.5 mL, 0.0395 mol), *O*-benzylhydroxylamine hydrochloride (6.3 g, 0.040 mol), EDC hydrochloride (4.54 g, 0.0395 mol), and DMAP (0.30 g, 0.0024 mol) were added to the reaction mixture in that order. The resulting mixture was stirred for 48 h at room temperature. DMF was removed under reduced pressure, and the resulting yellowish oil was diluted with ethyl acetate (50 mL). The organic phase was washed with a saturated $NaHCO_3$ solution (3 × 50 mL) and brine and then treated with anhydrous Na_2SO_4. The solvent was removed in vacuo and the product purified by flash column chromatography (silica gel, ethyl acetate/hexane 1/1 as the eluent). Pure compound **3** was isolated as a brownish powder (yield 2.74 g, 40%). ^1H NMR (400 MHz, δ, DMSO-d_6): 11.98 (1H, s, OBz-OH), 11.66 (1H, s, Ar-OH), 9.60 (1H, s, Ar-NH), 7.55 (1H, d, J = 8.7 Hz, Ar-6H), 7.42 (5H, m, OBz-H), 7.13 (1H, s, Ar-3H), 6.92 (1H, d, J = 8.7 Hz, Ar-1H), 4.92 (2H, s, OBz-CH_2). ESI-MS (QTOF, m/z): 737.28 ($[(M\text{-}H)_2Na]^-$). Anal. Found: C, 63.4; H, 6.3; N, 7.7. Calcd for $C_{19}H_{22}N_2O_5$: C, 63.7; H, 6.2; N, 7.8.

Synthesis of 4-Aminosalicyl-*O*-benzylhydroxamate (4). Compound **3** (2.09 g, 5.83 mmol) was dissolved in a dicholormethane/TFA mixture (1/1 v/v), and the solution was stirred for 2 h at room temperature. The solvent was removed in vacuo. The resulting oil was dissolved in 50 mL of ethyl acetate, washed with water (3 × 50 mL) and brine, and treated with anhydrous Na_2SO_4. The solvent was removed in vacuo, yielding compound **4** as a brownish powder (yield 1.9 g, 91%,). FT-IR (ATR, cm^{-1}): 2859, 2603, 1611, 1543, 1497, 1472, 1430, 1389, 1321, 1255, 1196, 1142, 1109, 1017, 974, 840, 906, 857, 823, 796, 734, 717, 695, 602, 570, 539, 517, 492. ^1H NMR (400 MHz, δ, DMSO-d_6): 7.49−7.26 (7H, m, OBz-H + Ar-1H), 6.03 (1H, d, J = 9.7 Hz, Ar-6H), 5.96 (s, 1H, Ar-3H), 5.79 (2H, s, Ar-NH_2), 4.88 (2H, s, Ar-NH_2). ESI-MS (QTOF, m/z): 281.22 ($[M + Na]^+$), 297.25 ($[M + K]^+$), 539.25 ($[M_2 + Na]^+$). Anal. Found: C, 65.4; H, 5.4; N, 10.6. Calcd for $C_{14}H_{14}N_2O_3$: C, 65.1; H, 5.5; N, 10.8.

Synthesis of 4-Aminosalicylhydroxamic Acid (H_3*p*-aShi, 5). Compound **4** (0.120 g, 0.464 mmol) was dissolved in 60 mL of methanol and hydrogenated in the presence of Pd/C (0.018 g, 15% w/w) under H_2 (p_{H2} = 30 psi) for 24 h. The catalyst was filtered off from the pale pink solution, the solvent removed in vacuo, and pure H_3*p*-aShi (**5**) isolated as a dark red powder (yield 0.050 g, 92%). ^1H NMR (400 MHz, δ, DMSO-d_6): 7.32 (1H, d, J = 8.6 Hz, Ar-6H), 6.00 (1H, dd, J = 8.6, $J_{1,3}$ = 2.2 Hz, Ar-3H), 5.94 (1H, d, J = 2.2 Hz, Ar-3H), 5.71 (2H, s, Ar-NH_2). ESI-MS (QTOF, m/z): 169.06 ($[M + H]^+$). Anal. Found: C, 50.3; H, 4.9; N, 16.4. Calcd for $C_7H_8N_2O_3$: C, 50.0; H, 4.8; N, 16.7.

Synthesis of Methyl 4-Iodosalicylate (7). Concentrated H_2SO_4 (2.02 mL) was slowly added at room temperature to a solution of 2-hydroxy-4-iodobenzoic acid (**6**; 4.00 g, 15.15 mmol) in dry methanol (37.2 mL). The reaction mixture was warmed to reflux for 12 h. After the mixture was cooled to room temperature, the solvent was removed to dryness. The crude product was dissolved in CH_2Cl_2 and washed with a saturated $NaHCO_3$ aqueous solution and then with brine. The organic phase was dried over anhydrous Na_2SO_4, filtered, and concentrated under vacuum to give product **7** as a white solid that was not further purified (yield 3.57 g, 85%). Mp: 64−65 °C. FT-IR (KBr, cm^{-1}): 3202, 2949, 2844, 1681. ^1H NMR (200 MHz, δ, $CDCl_3$): 3.98 (3H, s, CH_3), 7.27 (1H, dd, $J_{A,B}$ = 8.4, $J_{B,O}$ = 1.7 Hz, Ar-H_B), 7.44 (1H, d, $J_{C,O}$ = 1.6 Hz, Ar-H_C), 7.54 (1H, d, J = 8.4 Hz, Ar-H_A), 10.78 (1H, s, OH). $^{13}C\{^1H\}$ NMR (50 MHz, δ, $CDCl_3$): 52.69 (CH_3), 102.91 (I-C), 112.14 (Ar-C), 127.19 (Ar-CH), 128.84 (Ar-CH), 130.85 (Ar-CH), 161.69 (C-OH), 170.50 (C═O). HR ESI-MS (QTOF, m/z): 276.9353 ($[M^-]$).

Synthesis of Methyl 4-Iodo-2-(methoxymethoxy)benzoate (8). Methyl 4-iodosalicylate (**7**; 3.60 g, 13.04 mmol) was dissolved in dry DMF (36 mL) under a N_2 atmosphere. K_2CO_3 (7.20 g, 52.17 mmol) and chloromethyl methyl ether (2.08 mL, 27.39 mmol) were slowly added at room temperature, and the mixture was stirred for 15 h. The reaction mixture was then diluted with water and extracted with ethyl acetate. The organic phase was washed with brine, dried over anhydrous Na_2SO_4, filtered, and concentrated under vacuum, to give product **8** as a white solid (yield 4.00 g, 95%). Mp: 76−80 °C. FT-IR (KBr, cm^{-1}): 3104, 3080, 3013, 2969, 2914, 2858, 2833, 1721. ^1H NMR (200 MHz, δ, $CDCl_3$): 3.55 (3H, s, O-CH_3), 3.91 (3H, s, $COOCH_3$), 5.27 (2H, s, O-CH_2-O), 7.56−7.39 (2H, m, Ar-H_A, Ar-H_B), 7.61 (1H, s, Ar-H_C). $^{13}C\{^1H\}$ NMR (50 MHz, δ, $CDCl_3$): 52.36 (O-CH_3), 56.72 ($COOCH_3$), 95.42 (O-CH_2-O), 99.77 (I-C), 121.04 (C-CO), 125.85 (Ar-C), 131.12 (Ar-C), 132.68 (Ar-C), 157.09 (C-O), 166.23 (C═O). HR ESI-MS (QTOF, m/z): 344.9590 ($[M + Na]^+$).

Synthesis of Methyl-2-Hydroxy-4-(pyridin-4-yl)benzoate (9). A mixture of methyl 4-iodo-2-(methoxymethoxy)benzoate (**8**; 4.2 g, 13.04 mmol) and 4-pyridinylboronic acid (26.08 mmol, 3.21 g) in a Schlenk tube under nitrogen was dissolved with degassed solutions of toluene (110 mL), ethanol (22 mL), and aqueous Na_2CO_3 (2 M, 37 mL). After addition of $Pd(PPh_3)_4$ (1.50 g, 0.13 mmol) the reaction mixture was heated to 80 °C and stirred for 15 h. The reaction mixture was then cooled to room temperature, filtered over Celite, and concentrated under vacuum. The residue was diluted with ethyl acetate (50 mL) and extracted with HCl 1 M (4 × 50 mL). The aqueous phase was stirred for 2 h, basified with saturated $NaHCO_3$ solution to pH 5, and extracted with ethyl acetate (4 × 100 mL). The organic phase was dried over anhydrous Na_2SO_4 and concentrated under reduced pressure and the residue purified by silica gel column chromatography (dichloromethane/methanol 95/5), affording the product **9** as a light yellow solid (yield 2.64 g, 89%). Mp: 120−128 °C. FT-IR (KBr, cm^{-1}): 3150, 3063, 3015, 2961, 1677. ^1H NMR (200 MHz, δ, $CDCl_3$): 4.01 (3H, s, CH_3), 7.17 (1H, dd, $J_{A,B}$ = 8.3, $J_{B,O}$ = 1.8 Hz, Ar-H_B), 7.27 (1H, d, J = 1.7 Hz, Ar-H_C), 7.53 (2H, d, $J_{D,E}$ = 5.6 Hz, Py-H_D), 7.96 (1H, d, $J_{A,B}$ = 8.3 Hz, Ar-H_A), 8.72 (2H, d, J = 5.3 Hz, Py-H_E), 10.88 (1H, s, OH). $^{13}C\{^1H\}$ NMR (50 MHz, δ, $CDCl_3$): 52.69 (CH_3), 112.88 (C−CO), 116.19 (Ar-CH), 118.02 (Ar-CH), 121.86 (Py-CH), 130.94 (Ar-CH), 145.41 (Py-C), 147.11 (Ar-C), 150.54 (Py-CH), 162.08 (C-OH), 170.38 (C═O). HR ESI-MS (QTOF, m/z): 230.0813 ($[M + H]^+$).

Synthesis of 4-(Pyridin-4-yl)-salicylhydroxamic Acid (10, H_3*p*-pyShi). Hydroxylamine hydrochloride (1.81 g, 26 mmol) and NaOH (1.56 g, 39 mmol) were dissolved in water (60 mL), and a solution of methyl 2-hydroxy-4-(pyridin-4-yl)benzoate (**9**; 2.98 g, 13 mmol) in 1,4-dioxane (40 mL) was added dropwise. The mixture was stirred at room temperature for 12 h and then the solvent concentrated under vacuum. The product **10** was purified by crystallization from diethyl ether and obtained as a light yellow solid (yield 2.83 g, 95%). Mp: 178−184 °C. FT-IR (KBr, cm^{-1}): 3455, 3273, 1632, 1598. ^1H NMR (200 MHz, δ, DMSO-d_6): 7.00 (2H, m, ArH_C, Ar-H*B*), 7.64 (2H, d, J = 5.3 Hz, Py-H_D), 7.74 (1H, d, J = 7.8 Hz, Ar-H_A), 8.58 (2H, d, J = 5.3 Hz, Py-H_E). $^{13}C\{^1H\}$ NMR (50 MHz, δ, $CDCl_3$): 114.39 (Ar-CH), 115.19 (Ar-CH), 121.65 (Ar-

DOI: 10.1021/acs.cgd.8b01921
Cryst. Growth Des. 2019, 19, 1954−1964

C), 121.95 (Py-CH), 128.38 (Ar-CH), 138.08 (Py-C), 148.08 (Ar-C), 150.71 (Py-CH), 161.88 (C-OH), 165.19 (C=O). HR ESI-MS (QTOF, *m*/*z*): 231.0777 ($[M + H]^+$).

Synthesis of $Mn_{11}Shi_6$ (11), $Mn_{11}p$-aShi$_6$ (12), and $Mn_{11}p$-pyShi$_6$ (13). The three $Mn_{11}L_6$ metallacryptates (H_3L = H_3Shi, H_3p-aShi, H_3p-pyShi) were prepared using the following procedure. Manganese(II) acetate tetrahydrate (122 mg, 0.50 mmol), the ligand (32 mg of H_3Shi, 34 mg of H_3p-aShi, or 46 mg of H_3p-pyShi; 0.21 mmol), and sodium acetate trihydrate (28 mg, 0.2 mmol) were each dissolved in 2 mL of DMF. The three solutions were mixed with stirring in the following order: manganese(II) acetate, H_3L, and sodium acetate. The resulting dark brown solution was stirred for 4 h and then centrifuged to remove insoluble impurities. Slow evaporation of the supernatant at room temperature gave dark brown crystals suitable for XRD analysis within 4 weeks. Yields of compounds **11** and **13** were 28% and 2%, respectively. The synthesis of **12** was attempted several times, giving a few crystals of the compound only twice. From the other synthesis, a 12-MC-4 of formula $\{Mn^{II}(OAc)_2(O\text{-DMF})_5[12\text{-MC}_{Mn,p\text{-aShi}}\text{-}4]\}(DMF)_2$ was obtained (compound **12bis**). The structural description of this 12-MC-4 is provided as Supporting Information. The three complexes correspond to the following formulas: $Na_4[(Mn^{II})_2(Mn^{III})_9(\mu_3\text{-}O)_4(OAc)_9(Shi)_6(DMF)_3](DMF)_3(H_2O)_{6.75}$ (**11**), $Na_{3.5}H_{0.5}[(Mn^{II})_2(Mn^{III})_9(\mu_3\text{-}O)_4(OAc)_9(p\text{-aShi})_6](DMF)_{7.5}(H_2O)_6$ (**12**), and $H[(Mn^{II})_2(Mn^{III})_9(\mu_3\text{-}O)_4(OAc)_3(OH)_3(p\text{-pyShi})_6]\text{-}(H_2O)_6$ (**13**).[94] Several solvent molecules (not refined) are present in the channels of compounds **12** and **13**, as deduced by the presence of residual electron density. ESI-MS (QTOF, *m*/*z*) of a solution of **11** in methanol: *m*/*z* 1796 $[Mn_{11}(O)_4(Shi^{3-})_6(OAc)_3(OH)_3]^+$; 1810 $[Mn_{11}(O)_4(Shi^{3-})_6(OAc)_3(OH)_2(OMe)]^+$; 1824 $[Mn_{11}(O)_4(Shi^{3-})_6(OAc)_3(OH)(OMe)_2]^+$; 1838 $[Mn_{11}(O)_4(Shi^{3-})_6(OAc)_3(OMe)_3]^+$. ESI-MS (QTOF, *m*/*z*) of a solution of **12bis** in methanol: *m*/*z* 994 $[Mn_5(p\text{-aShi}^{3-})_4(OAc)]^+$. Compounds **12** and **13** were insoluble in all solvents suitable for ESI-MS characterization. Anal. Found for **11**: C, 34.5; H, 4.3; N, 6.5. Calcd for $C_{78}H_{106.5}Mn_{11}N_{12}Na_4O_{52.75}$: C, 34.0; H, 3.9; N, 6.1. Found for **12bis**: C, 40.5; H, 4.9; N, 13.2. Calcd for $C_{53}H_{75}Mn_5N_{15}O_{23}$: C, 40.7; H, 4.8; N, 13.4.

RESULTS AND DISCUSSION

Synthesis of the Ligands. The experimental procedure for preparing the ligand **5** (H_3p-aShi) was optimized by modifying a previously reported route for the synthesis of hydroxamic acids (Scheme 3).[79] The Boc protection of the amino group of the commercially available 4-aminosalicylic acid was followed by the condensation of the carboxylic function with *O*-benzylhydroxylamine. The *N*-Boc, *O*-Bz protected intermediate **3** was deprotected in two steps to yield the final H_3p-aShi (**5**) product.

Ligand **10** (H_3p-pyShi) could be obtained in very high yields via a four-step synthetic procedure from commercially available 4-iodosalicylic acid (**6**) (Scheme 4). After protection of the carboxylic acid as the methyl ester[80] and the phenol group as the methoxymethyl ether (MOM) (80% overall yield), Suzuki coupling[81,82] followed by an acidic workup allowed the insertion of the pyridine group and MOM protecting group removal, affording **9** in high yields (89%). The protection of the phenol and carboxylic acid functional groups was necessary to obtain an effective coupling reaction. Direct conversion in very high yields (95%) of the methyl ester **9** into the hydroxamic acid **10** was achieved using hydroxylamine hydrochloride and NaOH in a mixture of dioxane and water at room temperature.[81,82]

Scheme 3. Synthetic Route to H_3p-aShi (5) from 4-Aminosalicylic acid (1)[a]

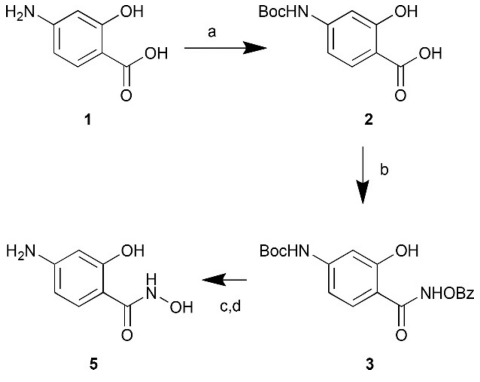

[a]Legend: (a) Boc_2O, NaOH, H_2O/EtOH, room temperature; (b) benzylhydroxylamine hydrochloride, triethylamine, EDC, DMAP, DMF, room temperature; (c) TFA, CH_2Cl_2; (d) H_2, Pd/C, MeOH.

Scheme 4. Synthetic Route to H_3p-pyShi (10) from 4-Iodosalicylic acid (6)[a]

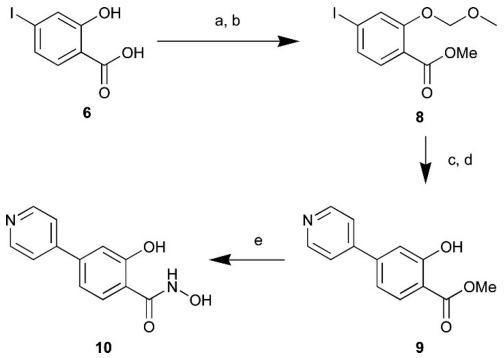

[a]Legend: (a) H_2SO_4, MeOH, reflux, N_2, 18 h; (b) MOM-Cl, K_2CO_3, DMF, room temperature, N_2, 12 h; (c) 4-Py-B(OH)$_2$, Pd(PPh$_3$)$_4$, Na_2CO_3 aqueous 2 M, toluene/EtOH, 100 °C, N_2; (d) HCl 1 M; (e) $NH_2OH{\cdot}HCl$, NaOH, H_2O/dioxane, room temperature.

General Description of the Metallacryptate Core in 11−13. The metallacryptates **11**−**13** were isolated after reaction of the ligands with manganese(II) acetate and sodium acetate in DMF. All three metallacryptates (MCr) **11**−**13** present a $[Mn^{II}]_2[Mn^{III}]_9$ polynuclear core, where nine Mn^{III} and two Mn^{II} are found (Figure 1). In all three compounds six hydroxamate ligands are present, which bridge between the

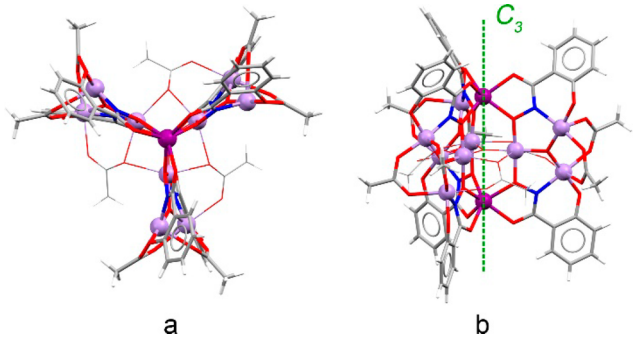

Figure 1. View of the $Mn_{11}L_6$ molecular unit of **11** along (a) and perpendicular (b) to the C_3 axis. Color scheme: light blue spheres, Mn^{III}; purple spheres, Mn^{II}. The acetate ions bridging between blades are represented with thin lines.

DOI: 10.1021/acs.cgd.8b01921
Cryst. Growth Des. 2019, 19, 1954−1964

manganese ions and give rise to a supramolecular complex that presents a crystallographic C_3 symmetry axis. Therefore, these assemblies are referred to as $Mn_{11}L_6$, where H_3L = H_3Shi, H_3*p*-aShi, H_3*p*-pyShi. The shape of the metallacryptate architecture is that of a three-bladed paddle wheel, where the blades are related by the crystallographic C_3 axis in all three compounds (Figures 1 and 2). For these reasons, we will first describe the structure of the blades and how they are connected together to give a metallacryptate motif.

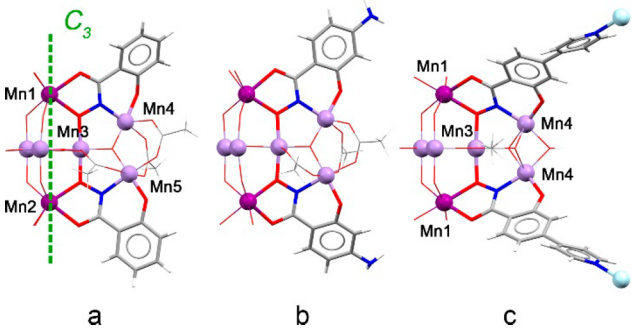

Figure 2. Representations of **11** (a), **12** (b), and **13** (c). The L^{3-} ligands are represented as sticks. Color scheme: light blue spheres, Mn^{III}; purple spheres, Mn^{II}. The cyan spheres in (c) represent Mn^{III} atoms of neighboring MCr molecules. The crystallographic C_3 axis is represented in green in (a) and is present in all three compounds. Labeling of atoms in (b) is the same as in (a).

The three molecules present very similar MCr architectures and similar connectivities of the blades, although with significant differences. Figure 2 shows how two L^{3-} ligands, three Mn^{III}, and one oxide ion are bound together. Two Mn^{II} are found at the apexes of the assembly, sitting on the C_3 axis, and coincide with the points of connections of the three MCr blades. The two L^{3-} ligands bridge between one Mn^{II} and one Mn^{III} ion through the bridging (N^-,O^-)-(O,O^-) bis-chelating mode known for this ligand. The Mn^{II} ions (Mn1 and Mn2) are coordinated to the hydroxamic (O,O^-) site of Shi^{3-} (purple spheres in Figure 2) in trigonal-prismatic (**11** and **12**) or octahedral (**13**) geometry. Conversely, the (N^-,O^-) site is occupied by a Mn^{III} ion (Mn4 and Mn5, light blue spheres in Figure 2). A third Mn^{III}/L^{3-} interaction involves the coordination of the hydroximate O^- atom to a Mn^{III} (Mn3) which is found in the center of the blade and which is part of the Mn_3O core of the MCr assembly (see below).

While the blades in compounds **11** and **12** are nearly planar, those of compound **13** are domed (see Figure S1 in the Supporting Information). Also, the blades in **13** bare two pyridyl groups that point away from the MCr unit and are coordinated to two neighboring molecules. These two structural features of the blades in **13** (i.e., concavity and presence of pyridyl groups) have profound consequences both on the molecular MCr architecture and on its assembly in the solid state, as discussed below.

In all three compounds, the three blades connect together ideally at the C_3 axis to form a MCr motif which has the connectivity Mn1−O−N−Mn4−O_{oxide}−Mn5−N−O−Mn2. This connectivity in compound **11** is represented as spheres in Figure 3a. Associated with this connectivity is the [1.1.1] ortho ester cryptand topology reported in Figure 3b.[83−85] This organic cryptand bears a C−CH_3 connection point rather than a nitrogen as in Lehn-type cryptands, allowing the first atom of

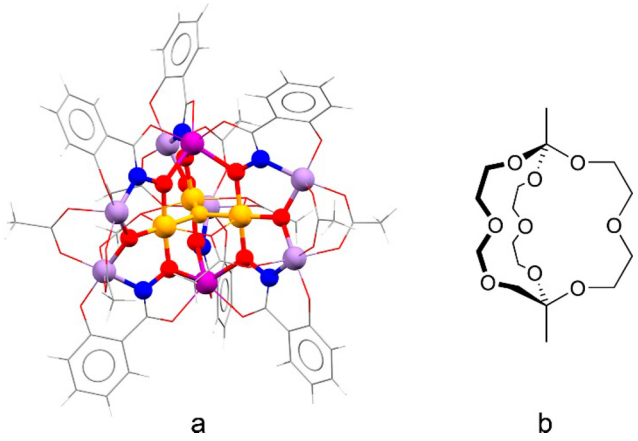

Figure 3. (a) Ball and stick representation of the metallacryptate connectivity in **11**. (b) Representation of a [*o*-Me_2-1.1.1] ortho ester cryptand. The connectivity in (a) is obtained from that in (b) by conceptually replacing the C−C bonds with Mn^{III}−N bonds and the C−CH_3 fragment with Mn^{II}. Color scheme: light blue spheres, Mn^{III}; purple spheres, Mn^{II}; blue spheres, N; red spheres, O. The $[Mn^{III}_3O]^{7+}$ unit is represented in yellow.

the arm to be an oxygen.[86] Finally, the MCr architecture sequesters a $[Mn^{III}_3O]^{7+}$ unit, which is represented in yellow in Figure 3a.

In this description of the MCr topology the oxide oxygen in the center of the blade is part of the MCr connectivity. Since an oxide ion is commonly found as a guest in supramolecular assemblies, the topology of our molecules is perhaps more appropriately described in terms of inverse metallacryptate (*inv*MCr) motifs, as represented in Figures S2 and S3 in the Supporting Information. For compounds **11** and **12**, the *inv*MCr connectivity is Mn1−O−N−Mn4−O−C−O−Mn5−N−O−Mn2 (Figure S2a). This description differs from the previous analysis in two aspects. On one hand, the connectivity does not pass through the oxide oxygen of the blade but rather through the O−C−O atoms of the carboxylates bridging between Mn4 and Mn5. From this perspective, the inverse metallacryptate topology is analogous with that of a Lehn-type [2.2.2] cryptand (Figure S2b), where the oxygen atoms are ideally substituted by Mn^{III}. In this inverse metallacryptate the sequestered host in the *inv*MCr is a $[Mn^{III}_3O_4]^+$ unit, which is reported in yellow in Figure S2a. Finally, all of the oxide ions in the molecule are part of the latter $[Mn^{III}_3O_4]^+$ guest unit.

In compound **13** the *inv*MCr connectivity is slightly different, since the two peripheral Mn^{III} of the blades (i.e., Mn4 and Mn5) are bridged by a hydroxide ion and not by carboxylates. Therefore, the analogous cryptand is still [2.2.2], but with a methylene spacer rather than a propylene (Figure S3 in the Supporting Information).

It must be underlined that, for both the metallacryptate and inverse MCr topologies, the connectivity does not correspond to $(Mn−N−O)_n$ repeats as found in normal metallacrowns and metallacryptates.[87] Actually, starting from Mn1 the O−N−Mn^{III} repeat inverts in correspondence with the carboxylates (compounds **11** and **12**) or the hydroxide bridging ligand (compound **13**). This type of connectivity in metallacrowns has been found for a Ln_2[14-MC-4] complex of Shi^{3-}, where the (Mn−N−O) repeat inverts in relationship to a Dy^{III} ion which is part of the metallacyclic ring.[31] Remarkably, also in this structure a hydroxide ion is a bridge between two ring

DOI: 10.1021/acs.cgd.8b01921
Cryst. Growth Des. 2019, 19, 1954−1964

Mn^{III} atoms, and it is located in correspondence to the inversion point of the repeats.[31]

Coordination Geometry of Mn^{II} and Mn^{III}. The molecular construct contains 11 Mn ions; the presence of 9 Mn^{III} and 2 Mn^{II} is in agreement with the bond valence sum.[88,89] The results of this analysis, together with a detailed discussion of the coordination environment of the different Mn ions, are reported as Supporting Information.

For all three MCr assemblies the nine Mn^{III} ions are located at the vertices of four interconnected $[Mn^{III}_3(\mu_3\text{-O})]^{7+}$ units (Figure 4). Therefore, three Mn_3O units other than that in the

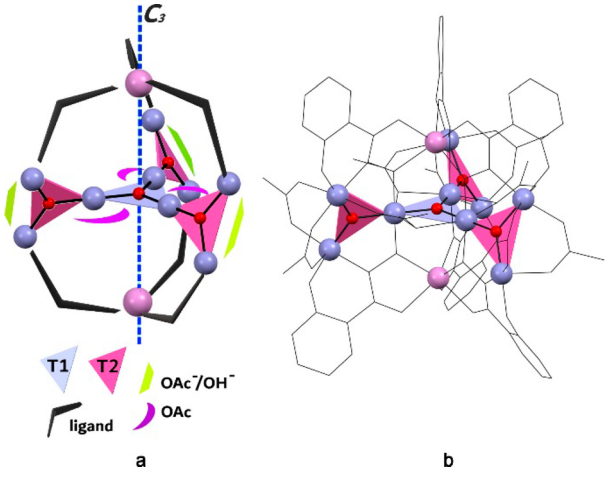

Figure 4. (a) Conceptual representation of the connectivity between Mn_3O units. The core T1 unit is represented as light blue triangles, and the peripheral T3 units are represented as magenta triangles. (b) Superimposition of the T1 and T3 representations over the crystal structure of **11**. The C_3 axis is represented in blue.

core are present in the structure, one for each blade. Figure 4a shows the conceptual arrangement of these units, represented as triangles. The core Mn_3O unit is indicated, as T1 and it is represented as a light purple triangle. In **11** and **12**, T1 coincides with a pseudosymmetry plane perpendicular to the C_3 axis, while in **13** it coincides with a crystallographic mirror element.

T1 is the *hub* Mn_3O unit to which the remaining three $[Mn^{III}_3\mu_3\text{-O}]^{7+}$ units are linked, as is indicated as T3 and represented in magenta in Figure 4. T3 units are connected to T1 by sharing a Mn^{III} at the vertex, and they are the *blade* Mn_3O units. T3 units are oriented almost perpendicularly to the plane of T1 and are almost parallel to the *paddle shaft*, which coincides with the 3-fold symmetry axis. In essence, in **11** and **12** each of the T3 motifs can be seen to originate from a substituted basic manganese acetate structure that has a core μ_3-O and six bridging carboxylates between the three Mn^{III} atoms (Mn3, Mn4, and Mn5).[90] Here four of the carboxylates on two of the Mn atoms are displaced by the bidentate L^{3-} ligand. The presence of axially elongated manganese(III) centers fully agrees with the presence of Mn^{III} ions with a high-spin d^4 configuration.[91,92]

Possibly more interesting than the coordination environment of the Mn^{III} is that of the Mn^{II}. The Mn^{II} atoms are located at the apexes of the MCr architecture (Mn1 and Mn2), they sit on the crystallographic C_3 axis, and they coordinate six oxygen atoms of three hydroxamate groups. The Mn−O distances are in the range 2.17−2.19 Å, consistent with typical Mn^{II}−O distances.[93] In **11** and **12** their coordination geometry is a distorted-trigonal prism, where the two triangular bases are perpendicular to the C_3 axis (Figure S4a,b). Actually, for Mn2 and Mn4, respectively, the rotation angles around the C3 axis of one base of the prism with respect to the other are 19 and 13° in **11** and 11 and 20° in **12**. Since the expected values are 0° for an ideal trigonal prism and 60° for an ideal trigonal antiprism or an octahedron, the geometry at the Mn^{II} centers in **11** and **12** is closer to a prism than to an antiprism. Conversely, the Mn^{II} atoms in **13** adopt a flattened-trigonal-antiprismatic coordination geometry (47° relative rotation angles of the bases, Figure S4c), likely the result of the presence of concave paddles. Notably, the prismatic coordination geometry of Mn1 and Mn2 in **11** and **12** is not accessible to high-spin Mn^{III} as a consequence of its d^4 configuration, while it can be adopted by a high-spin d^5 Mn^{II} ion.

Supramolecular Architectures in 11−13. The main structural core in all three reported structures is the MCr system, which can be viewed as a structural node in the supramolecular arrangement and crystal packing. We will provide here a description of the framework motifs that are generated by the $Mn_{11}L_6$ nodes assisted by the presence of sodium cations (in **11** and **12**), weak ligand interactions (in **12**), and a reticular coordination bond (in **13**).

In **11** each T3 blade is connected with the other two symmetry-related T3 blades by Na1 bridges, as shown in Figure S6. The $Mn_{11}L_6$ core is surrounded by six Na1 cations arranged in a flattened-octahedral geometry, whose connection with six distinct MCr nodes generates the overall framework (Figure 5). Along the direction of the C_3 axes, and interacting

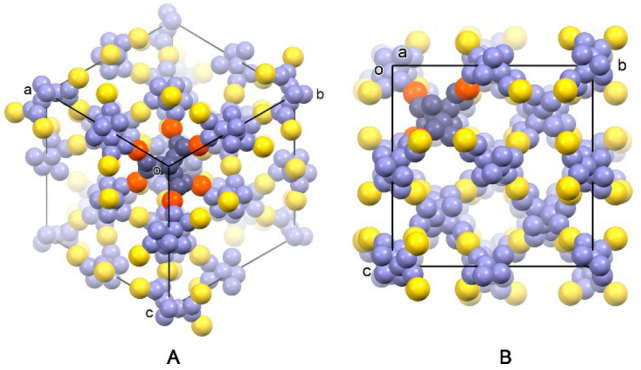

Figure 5. Representation of the framework of **11**. Only Mn^{III} (purple) and Na^{I} (yellow) atoms are depicted. Disordered Na2 and Na3 cations are not reported for clarity. The metal ions of the metallacryptate building block are highlighted in darker color tones. Views are given along the 111 direction (A) and along the *a* axis (B).

with the Mn^{II} ions (Mn1 and Mn2), are positioned disordered Na2 and Na3 sodium cations. Na2 and Na3 do not contribute to the construction of the framework, since they do not provide a bridging connection between symmetry-related $Mn_{11}L_6$ nodes. Water molecules of crystallization are found in the interstices of the framework.

Compound **12** exhibits an extensive packing arrangement of the $Mn_{11}L_6$ units (Figure 6). In more detail, the MCr units are connected through a dinuclear sodium−DMF moiety (Na2 and Na3 cations), resulting in a pillar that runs parallel to the *c* axis. The T3 blades then connect the pillars by means of the bridging Na1 cations and by extensive nets of hydrogen bonds between water molecules (O1w and O2w) and the peripheral amino groups of the *p*-aShi^{3-} ligand (Figure S7). The overall

DOI: 10.1021/acs.cgd.8b01921
Cryst. Growth Des. 2019, 19, 1954−1964

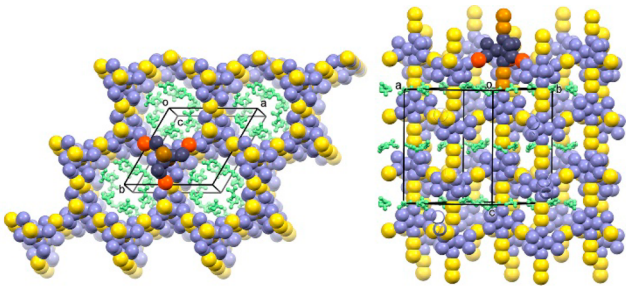

Figure 6. Representation of the framework of **12**. Mn (purple) and Na (yellow) atoms are depicted together with DMF solvent molecules (light green). The metal ions of the metallacryptate building block are highlighted in darker color tones. View are given along the *a* axis (A) and along the 110 direction (B).

arrangement leads to the formation of hexagonal channels, occupied by solvent molecules, which correspond to 39% of the unit cell volume (calculated with a sphere of 1.2 Å radius, Figure S8).

In compound **13**, the presence of the pyridyl fragment of *p*-pyShi^{3-} leads to the formation of an extensive 3D framework, whose nodes are represented by $Mn_{11}L_6$ units (Figure 7). Each node is bound to six neighboring nodes through 12 connections mediated by the pyridyl fragment. Six connections are diagonally directed above the T1 plane, and six connections are oriented below the same plane. The six connections above the T1 plane are eclipsed with respect to those below T1. More specifically, the interaction between the six $Mn_{11}L_6$ nodes occurs through a coordinative bond between the Mn4 ion of T3 and the nitrogen of the peripheral pyridyl group (Figure 7). The arrangement of the *p*-pyShi^{3-} ligands results in a hexagonal framework in a view along the *c* axis (Figure 8), which possesses a honeycomb arrangement of infinite, parallel channels. Also, along both the *a* and *b* directions smaller channels of trapezoidal sections are formed (Figure S9). These interpenetrated channels correspond to 55% of the unit cell volume.

For a comparison between compounds **12** and **13**, it is interesting to note that, although in low yields, the latter is selectively isolated from the mother liquors of crystallization. The same is not true for compound **12**, which has been isolated alternatively to a 12-MC-4 species from solutions obtained from the same experimental setup. Actually, while the architecture in **13** is organized in a way that possibly optimizes the interactions between the peripheral pyridyl groups and the Mn^{III} atoms of adjacent units, a similar situation is not observed in **12**. Rather, the analysis of **12** and **12bis** showed that in both structures the packing allows the NH_2 groups, for instance, to form hydrogen bonds that may contribute to stabilize the observed architectures. Therefore, we may put forward the hypothesis that the isolated architecture in **13** represents a quite stable one, while for the compounds obtained using *p*-aShi^{3-} the compounds **12** and **12bis** do not differ very significantly in terms of relative stability.

CONCLUSIONS

In this paper we showed that the use of Shi^{3-} ligands and manganese(II) acetate permits to isolation of stable metallacryptate supramolecules that are 3-fold symmetric and contain multiple Mn^{II} and Mn^{III} ions. These molecules are

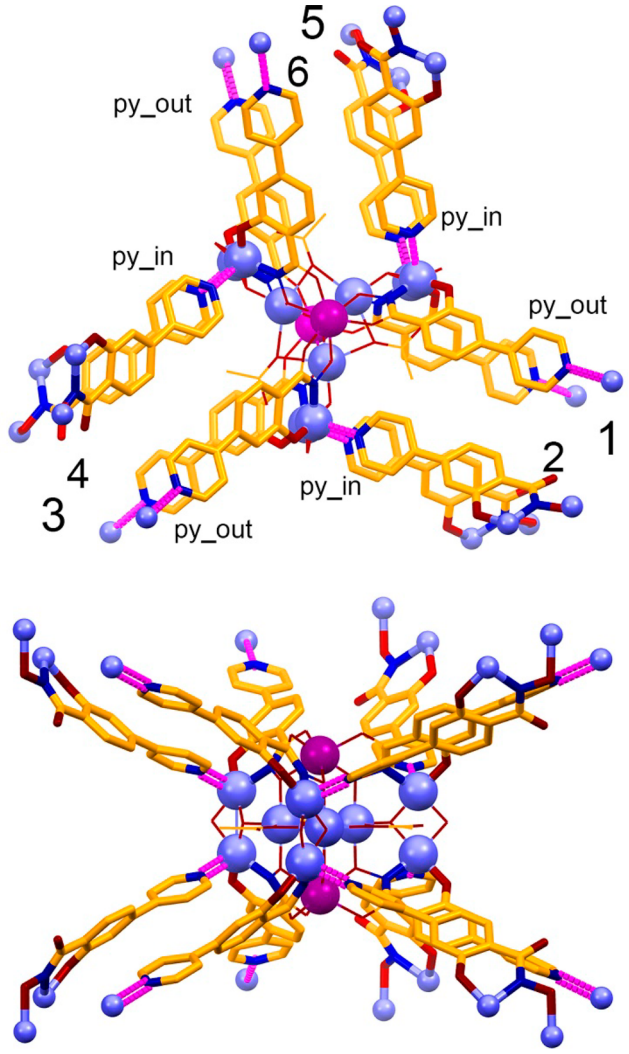

Figure 7. Two views of the $Mn_{11}L_6$ node in **13**, highlighting the 12 connections with 6 additional nodes (indicated with 1−6). Py_in and py_out indicate the pyridyl groups incoming and departing, respectively, to the indicated neighboring $Mn_{11}L_6$ node (as numbers).

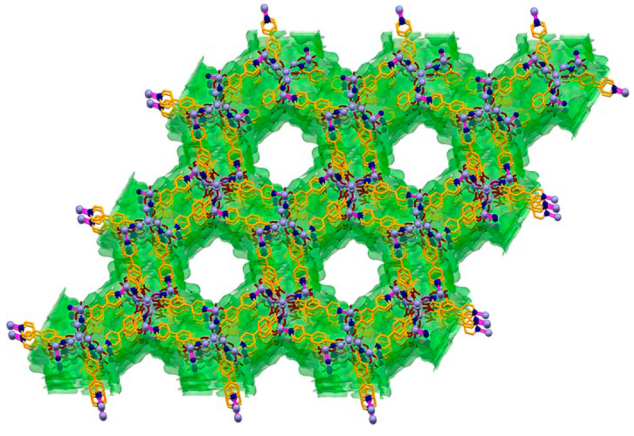

Figure 8. Channel-like cavities in **13**. Colors are as in Figure 7. The surface of the hexagonal channels is represented in green.

metallacrown-related analogues of organic cryptates and are the first presenting the same connectivity along the three arms.

The presence of an amino or a pyridyl substituent in position 4 on the Shi^{3-} aromatic ring has allowed us to prepare

DOI: 10.1021/acs.cgd.8b01921
Cryst. Growth Des. 2019, 19, 1954−1964

crystalline materials where the $Mn_{11}L_6$ units are arranged differently in the three dimensions. In the case of the ligands that we have examined, both the amino and the pyridyl functions are involved in the interaction between neighboring metallacryptate units. Perhaps more important, these groups correspond to the formation of porous structures, where chains of $Mn_{11}L_6$ units aligned along the 3-fold symmetry axis are assembled into honeycomb architectures. However, in the case of the *p*-aShi^{3-} ligand the units interact both through bridging Na^{I} ions and through an extensive net of hydrogen bonds that involve the NH_2 function and water molecules. However, it is with the ligand bearing the pyridyl group that a direct interaction between metallacryptates was obtained. Actually, the presence of that function allowed the formation of peripheral *p*-pyShi^{3-}–Mn^{III} interactions that resulted in the isolation of a porous metal–organic framework architecture.

In the future we aim to study these structures in terms both of their porosity and of the change in their magnetic properties as a function of the absorption of guest molecules such as gases or volatile liquids.

■ ASSOCIATED CONTENT

Supporting Information

The Supporting Information is available free of charge on the ACS Publications website at DOI: 10.1021/acs.cgd.8b01921.

Additional structural figures, valence bond sum analysis, structural description of **12bis**, NMR, FT-IR and ESI-MS characterization spectra, and crystallographic data (PDF)

Accession Codes

CCDC 1849184–1849186 and 1884452 contain the supplementary crystallographic data for this paper. These data can be obtained free of charge via www.ccdc.cam.ac.uk/data_request/cif, or by emailing data_request@ccdc.cam.ac.uk, or by contacting The Cambridge Crystallographic Data Centre, 12 Union Road, Cambridge CB2 1EZ, UK; fax: +44 1223 336033.

■ AUTHOR INFORMATION

Corresponding Authors

*V.L.P.: tel, +1 734 7631519; e-mail, vlpec@umich.edu.

*M.T.: tel, +39 0521 905424; e-mail, matteo.tegoni@unipr.it.

ORCID

Martina Quaretti: 0000-0001-7556-6031

Giulia Licini: 0000-0001-8304-0443

Luciano Marchiò: 0000-0002-0025-1104

Vincent L. Pecoraro: 0000-0002-1540-5735

Matteo Tegoni: 0000-0002-9621-0410

Present Address

‖Institut für Anorganische Chemie, Georg-August-Universität Göttingen, Tammannstraße 4, 37077 Göttingen, Germany.

Notes

The authors declare no competing financial interest.

■ ACKNOWLEDGMENTS

The research leading to these results has received funding from the European Community's Seventh Framework Programme (FP7/2013-2017) under grant agreement no. 611488. This work was supported by the National Science Foundation under grant no. CHE-1361799 to V.L.P. M.T. and V.L.P. thank the MAECI (Italian Ministry of Foreign Affairs and International Cooperation, Direzione Generale per la Promozione del Sistema Paese) for financial support through the bilateral Italy-USA project "Development of porous magnetic Metallacrowns for sensing applications". G.S. thanks the University of Padova for financial support (G.S. fellowship through Strategic Project NAMECA). M.T. and V.L.P. equally contributed to this research.

■ REFERENCES

(1) Zhou, H.-C.; Long, J. R.; Yaghi, O. M. Introduction To Metal–Organic Frameworks. *Chem. Rev.* **2012**, *112*, 673–674.

(2) Zhou, H.-C.; Kitagawa, S. Metal–Organic Frameworks (MOFs). *Chem. Soc. Rev.* **2014**, *43*, 5415–5418.

(3) Batten, S. R.; Champness, N. R.; Chen, X.-M.; Garcia-Martinez, J.; Kitagawa, S.; Öhrström, L.; O'Keeffe, M.; Suh, M. P.; Reedijk, J. Coordination Polymers, Metal–organic Frameworks And The Need For Terminology Guidelines. *CrystEngComm* **2012**, *14*, 3001–3004.

(4) Jiang, J.; Zhao, Y.; Yaghi, O. M. Covalent Chemistry Beyond Molecules. *J. Am. Chem. Soc.* **2016**, *138*, 3255–3265.

(5) Janiak, C.; Vieth, J. K. MOFs, MILs And More: Concepts, Properties And Applications For Porous Coordination Networks (PCNs). *New J. Chem.* **2010**, *34*, 2366–2388.

(6) Fujita, D.; Ueda, Y.; Sato, S.; Mizuno, N.; Kumasaka, T.; Fujita, M. Self-Assembly Of Tetravalent Goldberg Polyhedra From 144 Small Components. *Nature* **2016**, *540*, 563–566.

(7) Furukawa, H.; Cordova, K. E.; O'Keeffe, M.; Yaghi, O. M. The Chemistry And Applications Of Metal-Organic Frameworks. *Science* **2013**, *341*, 1230444.

(8) Cook, T. R.; Zheng, Y.-R.; Stang, P. J. Metal-Organic Frameworks And Self-Assembled Supramolecular Coordination Complexes: Comparing And Contrasting The Design, Synthesis, And Functionality Of Metal-Organic Materials. *Chem. Rev.* **2013**, *113*, 734–777.

(9) Tranchemontagne, D. J.; Mendoza-Cortes, J. L.; O'Keeffe, M.; Yaghi, O. M. Secondary Building Units, Nets And Bonding In The Chemistry Of Metal-Organic Frameworks. *Chem. Soc. Rev.* **2009**, *38*, 1257–1283.

(10) Atzeri, C.; Marchiò, L.; Chow, C. Y.; Kampf, J. W.; Pecoraro, V. L.; Tegoni, M. Design Of 2D Porous Coordination Polymers Based On Metallacrown Units. *Chem. - Eur. J.* **2016**, *22*, 6482–6486.

(11) Ostrowska, M.; Fritsky, I. O.; Gumienna-Kontecka, E.; Pavlishchuk, A. V. Metallacrown-Based Compounds: Applications In Catalysis, Luminescence, Molecular Magnetism, And Adsorption. *Coord. Chem. Rev.* **2016**, *327–328*, 304–332.

(12) Pavlishchuk, A. V.; Satska, Y.; Kolotilov, S. V.; Fritsky, I. Coordination Polymers And Oligonuclear Systems Based On Oximate Or Hydroxamate Building Blocks: Magnetic And Sorption Properties. *Curr. Inorg. Chem.* **2015**, *5*, 5–25.

(13) Lamberts, K.; Tegoni, M.; Jiang, X.; Kou, H.-Z.; Englert, U. Silver Complexation By Metallacryptates. *Dalton Trans.* **2016**, *45*, 284–295.

(14) Mezei, G.; Zaleski, C. M.; Pecoraro, V. L. Structural And Functional Evolution Of Metallacrowns. *Chem. Rev.* **2007**, *107*, 4933–5003.

(15) Tegoni, M.; Remelli, M. Metallacrowns Of Copper(II) And Aminohydroxamates: Thermodynamics Of Self Assembly And Host–guest Equilibria. *Coord. Chem. Rev.* **2012**, *256*, 289–315.

(16) Alexiou, M.; Katsoulakou, E.; Dendrinou-Samara, C.; Raptopoulou, C. P.; Psycharis, V.; Manessi-Zoupa, E.; Perlepes, S. P.; Kessissoglou, D. P. Di-2-Pyridyl Ketone Oxime In Zinc Chemistry: Inverse 12-Metallacrown-4 Complexes And Cationic Pentanuclear Clusters. *Eur. J. Inorg. Chem.* **2005**, *2005*, 1964–1978.

(17) Stemmler, A. J.; Kampf, J. W.; Pecoraro, V. L. Synthesis And Crystal Structure Of The First Inverse 12-Metallacrown-4. *Inorg. Chem.* **1995**, *34*, 2271–2272.

(18) Alexiou, M.; Dendrinou-Samara, C.; Raptopoulou, C. P.; Terzis, A.; Kessissoglou, D. P. From Monomer Zinc–Oxamato Complexes To Tetranuclear Inverse 12-Membered And Octanuclear 12-Membered Metallacrowns. *Inorg. Chem.* **2002**, *41*, 4732–4738.

DOI: 10.1021/acs.cgd.8b01921
Cryst. Growth Des. 2019, 19, 1954–1964

(19) Stamatatos, T. C.; Dionyssopoulou, S.; Efthymiou, G.; Kyritsis, P.; Raptopoulou, C. P.; Terzis, A.; Vicente, R.; Escuer, A.; Perlepes, S. P. The First Cobalt Metallacrowns: Preparation And Characterization Of Mixed-Valence Cobalt(II/III), Inverse 12-Metallacrown-4 Complexes. *Inorg. Chem.* **2005**, *44*, 3374−3376.
(20) Lah, M. S.; Gibney, B. R.; Tierney, D. L.; Penner-Hahn, J. E.; Pecoraro, V. L. The Fused Metallacrown Anion $Na_2([Na_{0.5}[Ga(Salicylhydroximate)]_4]_2(\mu_2\text{-}OH)_4)^-$ Is An Inorganic Analog Of A Cryptate. *J. Am. Chem. Soc.* **1993**, *115*, 5857−5858.
(21) Dendrinou-Samara, C.; Alexiou, M.; Zaleski, C. M.; Kampf, J. W.; Kirk, M. L.; Kessissoglou, D. P.; Pecoraro, V. L. Synthesis And Magnetic Properties Of A Metallacryptate That Behaves As A Single-Molecule Magnet. *Angew. Chem., Int. Ed.* **2003**, *42*, 3763−3766.
(22) Zaleski, C. M.; Depperman, E. C.; Dendrinou-Samara, C.; Alexiou, M.; Kampf, J. W.; Kessissoglou, D. P.; Kirk, M. L.; Pecoraro, V. L. Metallacryptate Single-Molecule Magnets: Effect Of Lower Molecular Symmetry On Blocking Temperature. *J. Am. Chem. Soc.* **2005**, *127*, 12862−12872.
(23) Lutter, J. C.; Eliseeva, S. V.; Kampf, J. W.; Petoud, S.; Pecoraro, V. L. A Unique Ln^{III}\{[3.3.1]Ga^{III} Metallacryptate\} Series That Possesses Properties Of Slow Magnetic Relaxation And Visible/Near-Infrared Luminescence. *Chem. - Eur. J.* **2018**, *24*, 10773−10783.
(24) Chow, C. Y.; Trivedi, E. R.; Pecoraro, V.; Zaleski, C. M. Heterometallic Mixed 3d-4f Metallacrowns: Structural Versatility, Luminescence, And Molecular Magnetism. *Comments Inorg. Chem.* **2015**, *35*, 214−253.
(25) Happ, P.; Plenk, C.; Rentschler, E. 12-MC-4 Metallacrowns As Versatile Tools For SMM Research. *Coord. Chem. Rev.* **2015**, *289−290*, 238−260.
(26) Jankolovits, J.; Andolina, C. M.; Kampf, J. W.; Raymond, K. N.; Pecoraro, V. L. Assembly Of Near-Infrared Luminescent Lanthanide Host(Host-Guest) Complexes With A Metallacrown Sandwich Motif. *Angew. Chem., Int. Ed.* **2011**, *50*, 9660−9664.
(27) Nguyen, T. N.; Chow, C. Y.; Eliseeva, S. V.; Trivedi, E. R.; Kampf, J. W.; Martinić, I.; Petoud, S.; Pecoraro, V. L. One-Step Assembly Of Visible And Near-Infrared Emitting Metallacrown Dimers Using A Bifunctional Linker. *Chem. - Eur. J.* **2018**, *24*, 1031−1035.
(28) Martinić, I.; Eliseeva, S. V.; Nguyen, T. N.; Pecoraro, V. L.; Petoud, S. Near-Infrared Optical Imaging Of Necrotic Cells By Photostable Lanthanide-Based Metallacrowns. *J. Am. Chem. Soc.* **2017**, *139*, 8388−8391.
(29) Trivedi, E. R.; Eliseeva, S. V.; Jankolovits, J.; Olmstead, M. M.; Petoud, S.; Pecoraro, V. L. Highly Emitting Near-Infrared Lanthanide "Encapsulated Sandwich" Metallacrown Complexes With Excitation Shifted Toward Lower Energy. *J. Am. Chem. Soc.* **2014**, *136*, 1526−1534.
(30) Chow, C. Y.; Eliseeva, S. V.; Trivedi, E. R.; Nguyen, T. N.; Kampf, J. W.; Petoud, S.; Pecoraro, V. L. Ga^{3+}/Ln^{3+} Metallacrowns: A Promising Family Of Highly Luminescent Lanthanide Complexes That Covers Visible And Near-Infrared Domains. *J. Am. Chem. Soc.* **2016**, *138*, 5100−5109.
(31) Boron, T. T.; Kampf, J. W.; Pecoraro, V. L. A Mixed 3d−4f 14-Metallacrown-5 Complex That Displays Slow Magnetic Relaxation Through Geometric Control Of Magnetoanisotropy. *Inorg. Chem.* **2010**, *49*, 9104−9106.
(32) Deb, A.; Boron, T. T.; Itou, M.; Sakurai, Y.; Mallah, T.; Pecoraro, V. L.; Penner-Hahn, J. E. Understanding Spin Structure In Metallacrown Single-Molecule Magnets Using Magnetic Compton Scattering. *J. Am. Chem. Soc.* **2014**, *136*, 4889−4892.
(33) Zaleski, C. M.; Tricard, S.; Depperman, E. C.; Wernsdorfer, W.; Mallah, T.; Kirk, M. L.; Pecoraro, V. L. Single Molecule Magnet Behavior Of A Pentanuclear Mn-Based Metallacrown Complex: Solid State And Solution Magnetic Studies. *Inorg. Chem.* **2011**, *50*, 11348−11352.
(34) Zaleski, C. M.; Depperman, E. C.; Kampf, J. W.; Kirk, M. L.; Pecoraro, V. L. Synthesis, Structure, And Magnetic Properties Of A Large Lanthanide−Transition-Metal Single-Molecule Magnet. *Angew. Chem., Int. Ed.* **2004**, *43*, 3912−3914.
(35) Zaleski, C. M.; Kampf, J. W.; Mallah, T.; Kirk, M. L.; Pecoraro, V. L. Assessing The Slow Magnetic Relaxation Behavior Of $Ln^{III}_4Mn^{III}_6$ Metallacrowns. *Inorg. Chem.* **2007**, *46*, 1954−1956.
(36) Boron, T. T.; Lutter, J. C.; Daly, C. I.; Chow, C. Y.; Davis, A. H.; Nimthong-Roldán, A.; Zeller, M.; Kampf, J. W.; Zaleski, C. M.; Pecoraro, V. L. The Nature Of The Bridging Anion Controls The Single-Molecule Magnetic Properties Of DyX_4M 12-Metallacrown-4 Complexes. *Inorg. Chem.* **2016**, *55*, 10597−10607.
(37) Chow, C. Y.; Bolvin, H.; Campbell, V. E.; Guillot, R.; Kampf, J. F.; Wernsdorfer, W.; Gendron, F. V.; Autschbach, J.; Pecoraro, V. L.; Mallah, T. Assessing The Exchange Coupling In Binuclear Lanthanide(III) Complexes And The Slow Relaxation Of The Magnetization In The Antiferromagnetically Coupled Dy_2 Derivative. *Chem. Sci.* **2015**, *6*, 4148−4159.
(38) Zaleski, C. M.; Depperman, E. C.; Kampf, J. W.; Kirk, M. L.; Pecoraro, V. L. Using $Ln^{III}[15\text{-}MC_{CuII(N)(S)\text{-}PheHA}\text{-}5]^{3+}$ Complexes To Construct Chiral Single-Molecule Magnets And Chains Of Single-Molecule Magnets. *Inorg. Chem.* **2006**, *45*, 10022−10024.
(39) Stemmler, A. J.; Kampf, J. W.; Kirk, M. L.; Atasi, B. H.; Pecoraro, V. L. The Preparation, Characterization, And Magnetism Of Copper 15-Metallacrown-5 Lanthanide Complexes. *Inorg. Chem.* **1999**, *38*, 2807−2817.
(40) Chow, C. Y.; Guillot, R.; Rivière, E.; Kampf, J. W.; Mallah, T.; Pecoraro, V. L. Synthesis And Magnetic Characterization Of Fe(III)-Based 9-Metallacrown-3 Complexes Which Exhibit Magnetorefrigerant Properties. *Inorg. Chem.* **2016**, *55*, 10238−10247.
(41) Atzeri, C.; Marzaroli, V.; Quaretti, M.; Travis, J. R.; Di Bari, L.; Zaleski, C. M.; Tegoni, M. Elucidation Of ^1H NMR Paramagnetic Features Of Heterotrimetallic Lanthanide(III)/Manganese(III) 12-MC-4 Complexes. *Inorg. Chem.* **2017**, *56*, 8257−8269.
(42) Pavlyukh, Y.; Rentschler, E.; Elmers, H. J.; Hübner, W.; Lefkidis, G. Magnetism Of Metallacrown Single-Molecule Magnets: From A Simplest Model To Realistic Systems. *Phys. Rev. B: Condens. Matter Mater. Phys.* **2018**, *97*, 214408.
(43) Lim, C.-S.; Tegoni, M.; Jakusch, T.; Kampf, J. W.; Pecoraro, V. L. Clarifying The Mechanism Of Cation Exchange In Ca(II)[15-$MC_{Cu(II)Ligand}$-5] Complexes. *Inorg. Chem.* **2012**, *51*, 11533−11540.
(44) Dallavalle, F.; Remelli, M.; Sansone, F.; Bacco, D.; Tegoni, M. Thermodynamics Of Self-Assembly Of Copper(II) 15-Metallacrown-5 Of Eu(III) Or Gd(III) With (*S*)-α-Alaninehydroxamic Acid In Aqueous Solution. *Inorg. Chem.* **2010**, *49*, 1761−1772.
(45) Tegoni, M.; Furlotti, M.; Tropiano, M.; Lim, C. S.; Pecoraro, V. L. Thermodynamics Of Core Metal Replacement And Self-Assembly Of Ca^{2+} 15-Metallacrown-5. *Inorg. Chem.* **2010**, *49*, 5190−5201.
(46) Grant, J. T.; Jankolovits, J.; Pecoraro, V. L. Enhanced Guest Affinity And Enantioselectivity Through Variation Of The Gd^{3+} [15-Metallacrown-5] Side Chain. *Inorg. Chem.* **2012**, *51*, 8034−8041.
(47) Jankolovits, J.; Kampf, J. W.; Maldonado, S.; Pecoraro, V. L. Voltammetric Characterization Of Redox-Inactive Guest Binding To Ln(III)[15-Metallacrown-5] Hosts Based On Competition With A Redox Probe. *Chem. - Eur. J.* **2010**, *16*, 6786−6796.
(48) Jankolovits, J.; Lim, C.-S. S.; Mezei, G.; Kampf, J. W.; Pecoraro, V. L. Influencing The Size And Anion Selectivity Of Dimeric Ln^{3+}[15-Metallacrown-5] Compartments Through Systematic Variation Of The Host Side Chains And Central Metal. *Inorg. Chem.* **2012**, *51*, 4527−4538.
(49) Jankolovits, J.; Cutland Van-Noord, A. D.; Kampf, J. W.; Pecoraro, V. L. Selective Anion Encapsulation In Solid-State Ln(III)[15-Metallacrown-5]$^{3+}$ Compartments Through Secondary Sphere Interactions. *Dalton Trans.* **2013**, *42*, 9803−9808.
(50) Lim, C.-S.; Jankolovits, J.; Zhao, P.; Kampf, J. W.; Pecoraro, V. L. Gd(III)[15-Metallacrown-5] Recognition Of Chiral α-Amino Acid Analogues. *Inorg. Chem.* **2011**, *50*, 4832−4841.
(51) Tegoni, M.; Tropiano, M.; Marchiò, L. Thermodynamics Of Binding Of Carboxylates To Amphiphilic Eu^{3+}/Cu^{2+} Metallacrown. *Dalton Trans.* **2009**, 6705−6708.
(52) Tegoni, M.; Remelli, M.; Bacco, D.; Marchiò, L.; Dallavalle, F. Copper(II) 12-Metallacrown-4 Complexes Of α-, β- And γ-Amino-

DOI: 10.1021/acs.cgd.8b01921
Cryst. Growth Des. 2019, 19, 1954−1964

hydroxamic Acids: A Comparative Thermodynamic Study In Aqueous Solution. *Dalton Trans.* **2008**, 2693−2701.
(53) Bodwin, J. J.; Cutland, A. D.; Malkani, R. G.; Pecoraro, V. L. The Development Of Chiral Metallacrowns Into Anion Recognition Agents And Porous Materials. *Coord. Chem. Rev.* **2001**, *216−217*, 489−512.
(54) Pavlishchuk, A. V.; Kolotilov, S. V.; Zeller, M.; Shvets, O. V.; Fritsky, I. O.; Lofland, S. E.; Addison, A. W.; Hunter, A. D. Magnetic And Sorption Properties Of Supramolecular Systems Based On Pentanuclear Copper(II) 12-Metallacrown-4 Complexes And Isomeric Phthalates: Structural Modeling Of The Different Stages Of Alcohol Sorption. *Eur. J. Inorg. Chem.* **2011**, *2011*, 4826−4836.
(55) Pavlishchuk, A. V.; Kolotilov, S. V.; Zeller, M.; Thompson, L. K.; Fritsky, I. O.; Addison, A. W.; Hunter, A. D. A Triple-Decker Heptadecanuclear $(Cu^{II})_{15}(Cr^{III})_2$ Complex Assembled From Pentanuclear Metallacrowns. *Eur. J. Inorg. Chem.* **2010**, *2010*, 4851−4858.
(56) Pavlishchuk, A. V.; Kolotilov, S. V.; Zeller, M.; Lofland, S. E.; Thompson, L. K.; Addison, A. W.; Hunter, A. D. High Nuclearity Assemblies And One-Dimensional (1D) Coordination Polymers Based On Lanthanide−Copper 15-Metallacrown-5 Complexes (Ln^{III} = Pr, Nd, Sm, Eu). *Inorg. Chem.* **2017**, *56*, 13152−13165.
(57) Pavlishchuk, A. V.; Kolotilov, S. V.; Zeller, M.; Lofland, S. E.; Kiskin, M. A.; Efimov, N. N.; Ugolkova, E. A.; Minin, V. V.; Novotortsev, V. M.; Addison, A. W. Supramolecular Maleate Adducts Of Copper(II) 12-Metallacrown-4: Magnetism, EPR, And Alcohol Sorption Properties. *Eur. J. Inorg. Chem.* **2017**, *2017*, 4866−4878.
(58) Pavlishchuk, A. V.; Kolotilov, S. V.; Zeller, M.; Thompson, L. K.; Addison, A. W. Formation Of Coordination Polymers Or Discrete Adducts Via Reactions Of Gadolinium(III)-Copper(II) 15-Metallacrown-5 Complexes With Polycarboxylates: Synthesis, Structures And Magnetic Properties. *Inorg. Chem.* **2014**, *53*, 1320−1330.
(59) Bodwin, J. J.; Pecoraro, V. L. Preparation Of A Chiral, 2-Dimensional Network Containing Metallacrown And Copper Benzoate Building Blocks. *Inorg. Chem.* **2000**, *39*, 3434−3435.
(60) Pecoraro, V. L.; Bodwin, J. J.; Cutland, A. D. Formation Of Chiral Solids Via A Molecular Building Block Approach. *J. Solid State Chem.* **2000**, *152*, 68−77.
(61) Lim, C.-S.; Jankolovits, J.; Kampf, J. W.; Pecoraro, V. L. Chiral Metallacrown Supramolecular Compartments That Template Nanochannels: Self-Assembly And Guest Absorption. *Chem. - Asian J.* **2010**, *5*, 46−49.
(62) Cutland-Van Noord, A. D.; Kampf, J. W.; Pecoraro, V. L. Preparation Of Resolved Fourfold Symmetric Amphiphilic Helices Using Chiral Metallacrown Building Blocks. *Angew. Chem., Int. Ed.* **2002**, *41*, 4667−4670.
(63) Wang, K.; Zou, H.-H.; Chen, Z.-L.; Zhang, Z.; Sun, W.-Y.; Liang, F.-P. A Series Of 3D Metal Organic Frameworks Based On [24-MC-6] Metallacrown Clusters: Structure, Magnetic And Luminescence Properties. *Dalton Trans.* **2014**, *43*, 12989.
(64) Aulakh, D.; Xie, H.; Shen, Z.; Harley, A.; Zhang, X.; Yakovenko, A. A.; Dunbar, K. R.; Wriedt, M. Systematic Investigation Of Controlled Nanostructuring Of Mn_{12} Single-Molecule Magnets Templated By Metal-Organic Frameworks. *Inorg. Chem.* **2017**, *56*, 6965−6972.
(65) Brunet, G.; Safin, D. A.; Jover, J.; Ruiz, E.; Murugesu, M. Single-Molecule Magnetism Arising From Cobalt(II) Nodes Of A Crystalline Sponge. *J. Mater. Chem. C* **2017**, *5*, 835−841.
(66) Campo, J.; Falvello, L. R.; Forcen-Vazquez, E.; Saenz de Pipaon, C.; Palacio, F.; Tomas, M. A Symmetric, Triply Interlaced 3-D Anionic MOF That Exhibits Both Magnetic Order And SMM Behaviour. *Dalton Trans.* **2016**, *45*, 16764−16768.
(67) Wang, H. H.; Yang, J.; Liu, Y. Y.; Song, S.; Ma, J. F. Heterotrimetallic Organic Framework Assembled With $Fe^{III}/Ba^{II}/Na^{I}$ And Schiff Base: Structure And Visible Photocatalytic Degradation Of Chlorophenols. *Cryst. Growth Des.* **2015**, *15*, 4986−4992.
(68) Aulakh, D.; Pyser, J. B.; Zhang, X.; Yakovenko, A. A.; Dunbar, K. R.; Wriedt, M. Metal-Organic Frameworks As Platforms For The Controlled Nanostructuring Of Single-Molecule Magnets. *J. Am. Chem. Soc.* **2015**, *137*, 9254−9257.
(69) *Single-Molecule Magnets and Related Phenomena*; Winpenny, R., Ed.; Springer-Verlag: Berlin/Heidelberg, 2006; Structure and Bonding Vol. *122*.
(70) Lis, T. Preparation, Structure, And Magnetic Properties Of A Dodecanuclear Mixed-Valence Manganese Carboxylate. *Acta Crystallogr., Sect. B: Struct. Crystallogr. Cryst. Chem.* **1980**, *36*, 2042−2046.
(71) Sessoli, R.; Gatteschi, D.; Caneschi, A.; Novak, M. A. Magnetic Bistability In A Metal-Ion Cluster. *Nature* **1993**, *365*, 141−143.
(72) *SMART (Control) And SAINT (Integration) Software*; Bruker AXS Inc.: Madison, WI, USA, 1994.
(73) *CrysAlis PRO*; Agilent Technologies Ltd: Yarnton, Oxfordshire, England, 2014.
(74) Sheldrick, G. M. *Area-Detector Absorption Correction*; Siemens Industrial Automation Inc.: Madison, WI, USA, 1996.
(75) Lausi, A.; Polentarutti, M.; Onesti, S.; Plaisier, J. R.; Busetto, E.; Bais, G.; Barba, L.; Cassetta, A.; Campi, G.; Lamba, D.; Pifferi, A.; Mande, S. C.; Sarma, D. D.; Sharma, S. M.; Paolucci, G. Status of the Crystallography Beamlines at Elettra. *Eur. Phys. J. Plus* **2015**, *130*, 43.
(76) Sheldrick, G. M. SHELXT − Integrated Space-Group And Crystal-Structure Determination. *Acta Crystallogr., Sect. A: Found. Adv.* **2015**, *71*, 3−8.
(77) Sheldrick, G. M. Crystal Structure Refinement With SHELXL. *Acta Crystallogr., Sect. C: Struct. Chem.* **2015**, *71*, 3−8.
(78) Macrae, C. F.; Bruno, I. J.; Chisholm, J. A.; Edgington, P. R.; McCabe, P.; Pidcock, E.; Rodriguez-Monge, L.; Taylor, R.; van de Streek, J.; Wood, P. A. Mercury CSD 2.0 − New Features For The Visualization And Investigation Of Crystal Structures. *J. Appl. Crystallogr.* **2008**, *41*, 466−470.
(79) Tegoni, M.; Ferretti, L.; Sansone, F.; Remelli, M.; Bertolasi, V.; Dallavalle, F. Synthesis, Solution Thermodynamics, And X-Ray Study Of Cu^{II} [12]Metallacrown-4 With GABA Hydroxamic Acid: An Unprecedented Crystal Structure Of A [12]MC-4 With A Gamma-Aminohydroxamate. *Chem. - Eur. J.* **2007**, *13*, 1300−1308.
(80) Sisco, S. W.; Moore, J. S. Directional Cyclooligomers Via Alkyne Metathesis. *J. Am. Chem. Soc.* **2012**, *134*, 9114−9117.
(81) Chowdhury, M. A.; Abdellatif, K. R. A.; Dong, Y.; Das, D.; Yu, G.; Velázquez, C. A.; Suresh, M. R.; Knaus, E. E. Synthesis And Biological Evaluation Of Salicylic Acid And N-Acetyl-2-Carboxybenzenesulfonamide Regioisomers Possessing A N-Difluoromethyl-1,2-Dihydropyrid-2-One Pharmacophore: Dual Inhibitors Of Cyclooxygenases And 5-Lipoxygenase With Anti-Inflammatory Ac. *Bioorg. Med. Chem. Lett.* **2009**, *19*, 6855−6861.
(82) Adamski-Werner, S. L.; Palaninathan, S. K.; Sacchettini, J. C.; Kelly, J. W. Diflunisal Analogues Stabilize The Native State Of Transthyretin. Potent Inhibition Of Amyloidogenesis. *J. Med. Chem.* **2004**, *47*, 355−374.
(83) Brachvogel, R.-C.; Maid, H.; von Delius, M. NMR Studies On Li^+, Na^+ And K^+ Complexes Of Orthoester Cryptand *o*-Me_2-1.1.1. *Int. J. Mol. Sci.* **2015**, *16*, 20641−20656.
(84) Brachvogel, R.-C.; Hampel, F.; von Delius, M. Self-Assembly Of Dynamic Orthoester Cryptates. *Nat. Commun.* **2015**, *6*, 7129.
(85) Low, H.; Mena-Osteritz, E.; von Delius, M. Self-Assembled Orthoester Cryptands: Orthoester Scope, Post-Functionalization, Kinetic Locking And Tunable Degradation Kinetics. *Chem. Sci.* **2018**, *9*, 4785−4793.
(86) Dietrich, B. Cryptands. In *Comprehensive Supramolecular Chemistry*; Gokel, G.W., Ed.; Elsevier: Oxford, 1996; Chapter 4, pp 153−211.
(87) Pecoraro, V. L.; Stemmler, A. J.; Gibney, B. R.; Bodwin, J. J.; Wang, H.; Kampf, J. W.; Barwinski, A.; Karlin, K. D. Metallacrowns: A New Class Of Molecular Recognition Agents. *Prog. Inorg. Chem.* **2007**, 83−177.
(88) Brown, I. D.; Altermatt, D. Bond-Valence Parameters Obtained From A Systematic Analysis Of The Inorganic Crystal Structure Database. *Acta Crystallogr., Sect. B: Struct. Sci.* **1985**, *41*, 244−247.
(89) Thorp, H. H. Bond Valence Sum Analysis Of Metal-Ligand Bond Lengths In Metalloenzymes And Model Complexes. *Inorg. Chem.* **1992**, *31*, 1585−1588.

DOI: 10.1021/acs.cgd.8b01921
Cryst. Growth Des. 2019, 19, 1954−1964

(90) Hessel, L. W.; Romers, C. The Crystal Structure Of "Anhydrous Manganic Acetate. *Recl. des Trav. Chim. des Pays-Bas* **1969**, *88*, 545−552.
(91) Avdeef, A.; Costamagna, J. A.; Fackler, J. P. Crystal And Molecular Structure Of Tris(Tropolonato)Manganese(III), Mn-$(O_2C_7H_5)_3$, A High-Spin Complex Having Structural Features Consistent With Jahn-Teller Behavior For Two Distinct MnO_6 Centers. *Inorg. Chem.* **1974**, *13*, 1854−1863.
(92) Fackler, J. P.; Avdeef, A. Crystal And Molecular Structure Of Tris(2,4-Pentanedionato)Manganese(III), $Mn(O_2C_5H_7)_3$, A Distorted Complex As Predicted By Jahn-Teller Arguments. *Inorg. Chem.* **1974**, *13*, 1864−1875.
(93) van Gorkum, R.; Buda, F.; Kooijman, H.; Spek, A. L.; Bouwman, E.; Reedijk, J. Trigonal-Prismatic Vs. Octahedral Geometry For Mn^{II} Complexes With Innocent Didentate Ligands: A Subtle Difference As Shown By XRD And DFT On $[Mn(acac)_2(bpy)]$. *Eur. J. Inorg. Chem.* **2005**, *2005*, 2255−2261.
(94) For each $Mn_{11}L_6$ in **12** and **13**, an excess of 0.5 and 1 negative charge was found. The structures exhibit a significant portion of the unit cells occupied by severely disordered solvent molecules that can easily accommodate the residual +0.5 or +1 charge in the form of disordered protons or sodium cations. This will result in the overall charge balance of the crystals. Here the formulas of **12** and **13** are reported by considering as counterions 0.5 and 1 proton per molecule, respectively.

DOI: 10.1021/acs.cgd.8b01921
Cryst. Growth Des. 2019, 19, 1954−1964